Excitonic effects in intraband quantum dot spectroscopy: Formation of bound continuum excitons

Sandra C. Kuhn and Marten Richter

Institut für Theoretische Physik, Nichtlineare Optik und Quantenelektronik, Technische Universität Berlin, Hardenbergstrasse 36, EW 7-1, 10623, Berlin, Germany

(Received 23 July 2014; revised manuscript received 2 September 2014; published 12 September 2014; publisher error corrected 30 April 2015)

We study intraband spectra, resulting from intraband transitions between the bound ground state of a semiconductor quantum dot and unbound continuum states in the host medium. The influence of excitonic coupling on these intraband absorption spectra and the formation of special excitons are discussed. Involving Coulomb coupled bound-to-continuum transitions, the spectra show the formation of bound excitons at the continuum edge and spectral shifts. The analyzed intraband absorption spectra exhibit different signatures for different initial carrier configurations.

DOI: 10.1103/PhysRevB.90.125308 PACS number(s): 73.20.Mf, 73.21.La, 78.67.−n

Semiconductor quantum dots (QDs) have attracted much attention due to their unique optical and electrical properties. They provide the basis for a variety of applications such as single photon emitters [1,2], light-emitting diodes [3], QD laser [4–6], and sources for nonclassical light [7,8]. Resulting from the crystal growth process, e.g., molecular beam epitaxy (MBE) [9] and metal-organic chemical-vapor deposition (MOCVD) [10], self organized QDs (fabricated by Volmer-Weber [11] or Stranski-Krastanow [11,12] growth) are embedded in two- or three-dimensional host materials. For these QD structures, the influence of Coulomb interactions on interband transitions inside the QD have been analyzed in detail, e.g., in Refs. [13,14] or by pump-probe experiments [15] and are well understood [16–19].

We study Coulomb effects on intraband transitions of carriers between bound (spatially confined) QD and unbound continuum states of the embedding material. The Coulomb effect on intraband transitions can play a role in a variety of experiments due to their relevance to the dephasing properties [20] of the QD states as well as for bound-to-continuum intraband spectroscopy [21].

For example, bound-to-continuum intraband transitions in self-assembled InAs/GaAs quantum dots (QDs) were studied experimentally [22] to realize high-quality optical devices operating at infrared wavelengths such as intermediate band solar cells [23], infrared emitter [24], and photodetectors [25,26]. In this article, we discuss Coulomb-induced effects on bound-to-continuum intraband absorption spectra between bound QD and continuum carriers (bulk or wetting layer) in optical spectra. In Refs. [27,28] calculations of the absorption coefficient for bound to continuum transitions excluding Coulomb interaction were presented. Experimentally, bound-to-continuum intraband absorption in InAs/GaAs self-assembled QDs have been observed by two-color photoexcitation spectroscopy [22,29] and using photoinduced absorption spectroscopy [30].

In contrast to free carrier theories [31], we present a theory based on the density matrix formalism [32] to calculate bound-to-continuum intraband absorption spectra including the Coulomb interaction and thus excitonic effects. We study several configurations of the initial occupations of the QD such as trions T^+ and T^-, biexciton BX, or exciton X [cf. Figs. 1(b) to 1(g)], resulting in characteristic spectral signatures. In particular, our results show signatures of an exciton consisting of a localized carrier inside the QD and a delocalized carrier of the continuum. The analysis in Ref. [33] suggests that bound-to-continuum excitons can play an important role in pump-probe experiments.

As a model system we use a self-organized InAs QD with spin-degenerated states i in each band embedded in GaAs bulk material [cf. Fig. 1(a)], here for the case without a wetting layer. For both the conduction band and valence band, continuum states and bound states localized in the QD exist. The continuum bulk states are approximately characterized by a wave vector $\mathbf{k}$ and a spin σ. For simplicity, we select QDs with one bound state i. QDs with several bound states can be considered analogous, including the extended QD states in the $\mathbf{k}$ index. The proposed study is also applicable to other materials (or other nanostructures embedded in a continuum).

We denote the ground state of the QD continuum system by $|\Phi_0\rangle$. For a measurement of a bound-to-continuum intraband absorption spectrum, occupied bound conduction (valence) band states and the ability to optically probe bound-continuum transitions are necessary. Therefore, before the system is optically tested with respect to absorption at least one electron (hole) is prepared in a bound state of the QD. Several initial configurations can be investigated, cf. Figs. 1(b) to 1(g). These different occupations may be prepared differently, e.g., by a pump pulse [19,34–36] or by doped QDs. In the configuration depicted in Fig. 1(a), the QD can be initially prepared by a resonant pump pulse with an electron and hole in the two bound states (the QD exciton X), cf. Fig. 1(c). The final initial occupations $|c\rangle$, which are probed afterward by the test pulse, and are constructed by

$$\begin{aligned} |c\rangle &:= \left|n^e_{i,\uparrow},n^e_{i,\downarrow},n^h_{i,\uparrow},n^h_{i,\downarrow}\right\rangle \\ &:= (h^\dagger_{i,\downarrow})^{n^h_{i,\downarrow}}(h^\dagger_{i,\uparrow})^{n^h_{i,\uparrow}}(e^\dagger_{i,\downarrow})^{n^e_{i,\downarrow}}(e^\dagger_{i,\uparrow})^{n^e_{i,\uparrow}}|\Phi_0\rangle, \end{aligned} \tag{1}$$

from the ground state $|\Phi_0\rangle$ of the system with no electron or hole carriers. Here $e^\dagger_{i(\mathbf{k}),\sigma}$ ($e_{i(\mathbf{k}),\sigma}$) are the creation (annihilation) operators for electrons and $h^\dagger_{i(\mathbf{k}),\sigma}$ ($h_{i(\mathbf{k}),\sigma}$) for holes of the QD state i (or for the $\mathbf{k}$th continuum state) with the spin σ, respectively. $|n^e_{i,\uparrow},n^e_{i,\downarrow},n^h_{i,\uparrow},n^h_{i,\downarrow}\rangle$ are Fock states for the electrons and holes with the occupation numbers $n^{e(h)}_{i,\sigma} = 0,1$.

The intraband electron transition $e^\dagger_{\mathbf{k},\sigma}e_{i,\sigma}$ occurs between the QD ground state i and the continuum states $\mathbf{k}$ of the

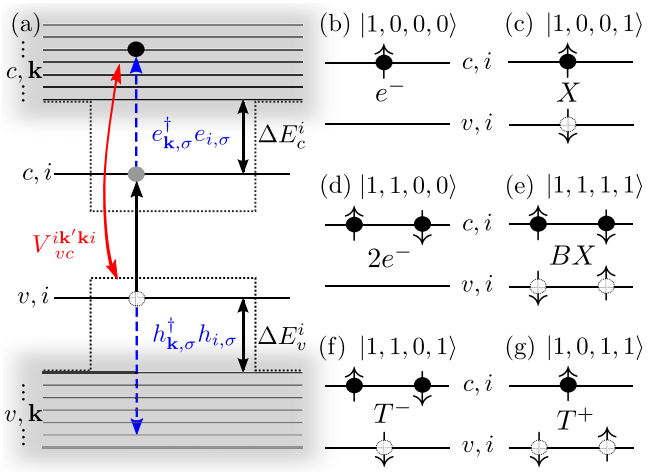

FIG. 1. (Color online) (a) Level scheme of the QD continuum model: The bulk states have a crystal momentum $\mathbf{k}$ and a spin σ. i represents the spin-degenerated QD states. The energy difference between the QD state i and the lowest (highest) energy bulk state in the conduction (valence) band is ΔE^i_c (ΔE^i_v). The intraband transitions between the dot levels and the bulk states $e^\dagger_{\mathbf{k},\sigma}e_{i,\sigma}$ and $h^\dagger_{\mathbf{k},\sigma}h_{i,\sigma}$ are tested by a probe pulse. The electron in the continuum and the localized hole in the QD couple via Coulomb interaction $V^{i\mathbf{k}'\mathbf{k}i}_{vc}$. Initial occupations $|n^e_{i,\uparrow},n^e_{i,\downarrow},n^h_{i,\uparrow},n^h_{i,\downarrow}\rangle$ of the QD. (b) Doped with one electron e^-, (c) one exciton X, (d) doped with two electrons $2e^-$, (e) biexcitons BX, (f) negative-charged trion T^-, and (g) positive-charged trion T^+.

bulk, cf. dashed lines in Fig. 1. The intraband transition changes the system from the initial state $|c\rangle$ into an excited state $|\mathbf{k}\sigma\rangle := e^\dagger_{\mathbf{k},\sigma}e_{i,\sigma}|c\rangle$. In the density matrix formalism the expectation value of these intraband transitions are described by the density matrix elements $\langle c|\rho|\mathbf{k}\sigma\rangle$ where ρ denotes the statistical operator. Interband transitions between bound valence band and conduction band states start at higher energies. Therefore, they are separated from the intraband spectrum and can be neglected in its calculation.

The spectral range of interest is given by the energy difference between the bound QD state and the lowest (highest) continuum state in the conduction (valence) band ΔE^i_c (ΔE^i_v), considering the excitonic shifts.

The spectral intraband absorption, which is tested by a probe pulse $\mathbf{E}(\omega)=\mathcal{E}(\omega)\mathbf{e}_\xi$ with the polarization direction $\mathbf{e}_\xi$, can be calculated via the macroscopic polarization [37] $\mathcal{P}_{\text{intra}}(\omega)=\mathbf{P}_{\text{intra}}(\omega)\cdot\mathbf{e}_\xi$:

$$\alpha^{(e/h)}(\omega)=\frac{\omega}{nc\epsilon_0}\text{Im}\left[\frac{\mathcal{P}^{(e/h)}_{\text{intra}}(\omega)}{\mathcal{E}(\omega)}\right]. \tag{2}$$

Here n is the constant background refractive index around the relevant transition frequencies, ϵ_0 the vacuum permittivity, and c the speed of light. Equation (2) holds for electron and hole transitions.

The contributions from hole and electron intraband transitions occur independently and do not depend on the other carrier system [27]. Therefore, it is possible to split up the intraband absorption spectrum $\alpha(\omega)$ into an electron $\alpha^e(\omega)$ and a hole contribution $\alpha^h(\omega)$. All of the following results are qualitatively similar for $\alpha^e(\omega)$ and $\alpha^h(\omega)$ and both are usually spectrally well separated; here we present only $\alpha^e(\omega)$. The excitation pulse $\mathbf{E}(t)=\mathcal{E}(t)\mathbf{e}_\xi$ (polarization direction $\mathbf{e}_\xi$) induces the macroscopic electron polarization $\mathcal{P}^e_{\text{intra}}(t)$:

$$\mathcal{P}^e_{\text{intra}}(t)=N_{\text{QD}}\sum_{\mathbf{k},\sigma}d^{\mathbf{k}i}_c\langle c|\rho|\mathbf{k}\sigma\rangle(t)+\text{c.c.}, \tag{3}$$

where N_{QD} denotes the QD volume density. $d^{\mathbf{k}i}_\lambda$ are the intraband dipole matrix elements, respectively, in the $\mathbf{e}_\xi$ direction and with band index $\lambda\in\{c,v\}$:

$$d^{\mathbf{k}i}_{c(v)}=q\int\phi^{e(h),*}_{\mathbf{k}}(\mathbf{r})r_\xi\phi^{e(h)}_i(\mathbf{r})d\mathbf{r}, \tag{4}$$

here $\phi^{e(h)}_{i(\mathbf{k})}(\mathbf{r})$ are the electron (hole) envelope wave function [38] of the QD state i or of the continuum state $\mathbf{k}$, $r_\xi=\mathbf{e}_\xi\cdot\mathbf{r}$, and q is the electron charge.

The temporal evolution of the density matrix elements $\langle c|\rho|\mathbf{k}\sigma\rangle$ is calculated via the Liouville–von Neumann equation

$$\partial_t\langle c|\rho|\mathbf{k}\sigma\rangle=-\frac{i}{\hbar}\langle c|[H,\rho]|\mathbf{k}\sigma\rangle. \tag{5}$$

The total Hamiltonian H consists of the single-particle contribution H_0, the interaction of electrons, and the classical light field H_L and the Coulomb-interaction H_C:

$$\begin{aligned}H_0=&\sum_\sigma(\epsilon_{c,i}e^\dagger_{i,\sigma}e_{i,\sigma}+\epsilon_{v,i}h^\dagger_{i,\sigma}h_{i,\sigma})\\&+\sum_{\mathbf{k},\sigma}(\epsilon_{c,\mathbf{k}}e^\dagger_{\mathbf{k},\sigma}e_{\mathbf{k}\sigma}+\epsilon_{v,\mathbf{k}}h^\dagger_{\mathbf{k},\sigma}h_{\mathbf{k},\sigma}),\end{aligned} \tag{6}$$

where $\epsilon_{\lambda,i(\mathbf{k}),\sigma}$ is the single-particle energy of the bound QD state i and the unbound continuum states $\mathbf{k}$ including Coulomb renormalization with the spin σ and the band index $\lambda\in\{c,v\}$. In our model, the spin-up and spin-down QD states of the same band are assumed to be energetically degenerate $\epsilon_{\lambda,i(\mathbf{k}),\uparrow}=\epsilon_{\lambda,i(\mathbf{k}),\downarrow}=\epsilon_{\lambda,i(\mathbf{k})}$.

The intraband interaction of the carriers with the external light field $\mathbf{E}(t)=\mathcal{E}(t)\mathbf{e}_\xi$ with the polarization direction $\mathbf{e}_\xi$ is in the dipole approximation given by

$$H_{\text{L}}=-\sum_{\mathbf{k},\sigma}\left(d^{i\mathbf{k}}_c\mathcal{E}(t)e^\dagger_{i,\sigma}e_{\mathbf{k},\sigma}+d^{i\mathbf{k}}_v\mathcal{E}(t)h^\dagger_{i,\sigma}h_{\mathbf{k},\sigma}\right)+\text{h.a.} \tag{7}$$

As the final contribution of the Hamiltonian we add the Coulomb interaction, which in the electron hole picture reads [15]

$$\begin{aligned}H_C=\frac{1}{2}\sum_{\mathbf{s}}\big(&V^{s_1s_2s_3s_4}_{cc}\;e^\dagger_{s_1}e^\dagger_{s_2}e_{s_3}e_{s_4}+V^{s_1s_2s_3s_4}_{vv}\;h^\dagger_{s_3}h^\dagger_{s_4}h_{s_1}h_{s_2}\\&-2V^{s_1s_2s_3s_4}_{vc}\;e^\dagger_{s_2}h^\dagger_{s_4}h_{s_1}e_{s_3}\big),\end{aligned} \tag{8}$$

where s_1,s_2,s_3, and s_4 are multi-indices of the energy levels of the system, consisting of index i for bound QD states or continuum states $\mathbf{k}$ and spin σ. Since processes induced by the Auger Coulomb elements (e.g., $s_1=i$, $s_2=i$, $s_3=i$, and $s_4=\mathbf{k}$) create intraband polarizations at different energies than intraband bound continuum transitions in the absorption spectrum or are nonenergy conserving, they are not included in the Hamiltonian Eq. (8). Using the Bloch waves approach for the single-particle wave functions, the Coulomb coupling

elements $V^{s_1s_2s_3s_4}_{\lambda_1\lambda_2}$ in zero-order Taylor expansion of the Coulomb potential $W(\mathbf{r}) = e^2/(4\pi\epsilon_0\epsilon_r r)$ read:

$$V^{s_1s_2s_3s_4}_{\lambda_1\lambda_2} = \iint \phi^*_{\lambda_1,s_1}(\mathbf{r})\phi^*_{\lambda_2,s_2}(\mathbf{r}')W(|\mathbf{r}-\mathbf{r}'|) \times \phi_{\lambda_2,s_3}(\mathbf{r}')\phi_{\lambda_1,s_4}(\mathbf{r})d\mathbf{r}d\mathbf{r}', \quad (9)$$

where $\phi_{\lambda,s}(\mathbf{r})$ denote the envelope wave functions and $\epsilon_r = 12.53$ is the relative permittivity of GaAs [39]. Since the QD wave function is localized, screening is probably not as important as for continuum excitons and is only considered by ϵ_r.

Using Eqs. (6) to (8) in Eq. (5), the dynamics of $\langle c|\rho|\mathbf{k}\uparrow\rangle$ ($\langle c|\rho|\mathbf{k}\downarrow\rangle$ analog) is calculated in Eq. (10), which is only valid for linear optics:

$$\begin{aligned}\partial_t\langle c|\rho|\mathbf{k}\uparrow\rangle &= \frac{1}{i\hbar}\Big\{\big[\epsilon_{c,i}n^e_{i,\uparrow} - \epsilon_{c,\mathbf{k}}\big(1-n^e_{\mathbf{k},\uparrow}\big) - i\gamma\big]\langle c|\rho|\mathbf{k}\uparrow\rangle \\ &+ \left(V^{iiii}_{cc}\ n^e_{i,\uparrow}n^e_{i,\downarrow} - \sum_\sigma V^{iiii}_{vc}\ n^e_{i,\uparrow}n^h_{i,\sigma}\right)\langle c|\rho|\mathbf{k}\uparrow\rangle \\ &+ d^{i\mathbf{k}}_c\ \mathcal{E}(t)n^e_{i,\uparrow}\big(1-n^e_{\mathbf{k},\uparrow}\big)\langle c|\rho|c\rangle \\ &+ \left(\sum_{\mathbf{k}',\sigma} V^{i\mathbf{k}'\mathbf{k}i}_{vc}n^h_{i,\sigma} - \sum_{\mathbf{k}'} V^{i\mathbf{k}'\mathbf{k}i}_{cc}n^e_{i,\downarrow}\right)\big(1-n^e_{\mathbf{k},\uparrow}\big)\langle c|\rho|\mathbf{k}'\uparrow\rangle \\ &- \sum_{\mathbf{k}'} V^{i\mathbf{k}'i\mathbf{k}}_{cc}\ n^e_{i,\uparrow}\big(1-n^e_{\mathbf{k},\uparrow}\big)\langle c|\rho|\mathbf{k}'\downarrow\rangle\Big\} \quad (10)\end{aligned}$$

introducing a phenomenological dephasing [40] γ. In Eq. (10) we neglect the coupling of $\langle c|\rho e^\dagger_{\mathbf{k},\sigma}e_{i,\sigma}|c\rangle = \langle c|\rho|\mathbf{k}\sigma\rangle$ to $\langle c|\rho h^\dagger_{\mathbf{k},\sigma}h_{i,\sigma}|c\rangle$ due to the different energies of the bound-to-continuum intraband transitions for electrons and holes. The objective of our theory is the calculation of linear absorption spectra. Therefore, higher-order contributions to the electrical field are not included in Eq. (10). Without electrically injected carriers there is no electron (hole) occupation in the bulk conduction (valence) band: $n^e_{\mathbf{k},\sigma} = 0$.

To solve Eq. (10) the Coulomb coupling elements $V^{s_1s_2s_3s_4}_{\lambda_1\lambda_2}$ and the dipole moments $d^{i\mathbf{k}}_\lambda$ are needed. Their calculation requires the QD and the continuum wave functions, cf. Eqs. (4) and (9). Therefore, we assume spherical QDs and use the ansatz $\phi(\mathbf{r}) = Y^m_l(\vartheta,\varphi)R_l(r)$ for the envelope part of the wave function. The radial Schrödinger equation can be solved for $R_l(r)$ numerically using a finite element method (FEM) solver [41] and assuming a QD confinement potential, e.g., an inverse hyperbolic secant potential[1] $V(r) = -\frac{V_0}{\cosh^2(\frac{r}{a})}$ with height V_0 and extension a.

We studied several confinement potential parameters a and V_0 with qualitatively similar results. Here, we only present as an example the results for shallow QDs with one bound state in the conduction band. For these QDs we choose parameters[2] for V_0 and a, resulting in a QD confinement potential and a QD electron ground-state wave function with a localization length of $r_0 = 3.7$ nm (depicted in Fig. 2). Typical values of the localization length r_0 of self-assembled QDs are between [42–45] $r_0 = 3$ and 5.5 nm. The localized electron state is separated from the continuum of delocalized states by [42–44] $\Delta E^i_c = 50$ meV. Large QDs with deep QD confinement potentials can be treated in an analogous way. In addition to the bound-to-continuum intraband transition also bound-to-bound intraband transitions occur inside the QD for deeper QDs, resulting in additional sharp absorption peaks. The angular momentum of the conduction band ground-state envelope functions of the QD is $l = 0$. Only the continuum (or excited QD) wave functions with $l = 1$ are contributing, cf. Eq. (4), since selection rule $\Delta l = 1$ holds for intraband transitions.

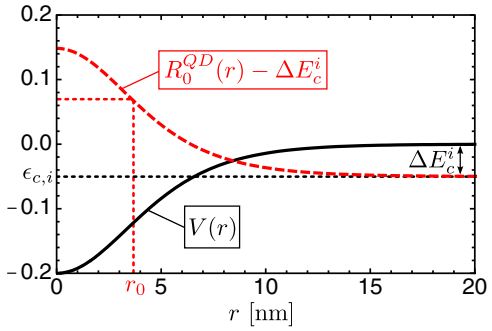

FIG. 2. (Color online) Model QD confinement potential $V(r)$ with $\Delta E^i_c = 50$ meV and the corresponding electron QD ground-state wave function $R^{\mathrm{QD}}_0(r)$ with $r_0 = 3.7$ nm.

In Fig. 3 intraband absorption spectra for several initial configurations $|c\rangle$ [as depicted in Figs. 1(b) to 1(g)] prepared before the test pulse are shown. Since the Coulomb interaction is a two-particle interaction, it influences the spectrum only if more than one carrier is present in the initial configuration. Therefore for a single electron e^- in the QD [Fig. 1(b)] the intraband absorption spectrum is not influenced by Coulomb-induced effects. The corresponding spectrum is shown as e^- in Fig. 3. Here, the bound-to-continuum intraband absorption starts at the energy difference $\Delta E^i_c = 50$ meV of the single-particle energies between the QD conduction band ground state and the energetically closest continuum state. The shape of the absorption peaks is determined by the shape of the QD conduction band ground bound state wave function [27]: The spectrum reaches a maximum and then decreases since the QD wave function also decreases.

If more than one carrier is present in the system, Coulomb processes occur between the carriers. The Coulomb interaction results in joint different spectral signatures, depending on the initial occupations of the QD (before the probe pulse tests the intraband transitions). In Figs. 1(c) to 1(g) the investigated initial configurations are depicted. Three significant Coulomb

[1]We assume typical parameters for the effective mass of GaAs in units of m^*_0 such as $m^*_e = 0.065$ for electrons and $m^*_{hh} = 0.5$ for holes.

[2]The potential height for the conduction (valence) band is assumed to be $V^c_0 = 0.2$ eV ($V^v_0 = 0.025$ eV) and the extension of the confinement potential is $a = 5$ nm.

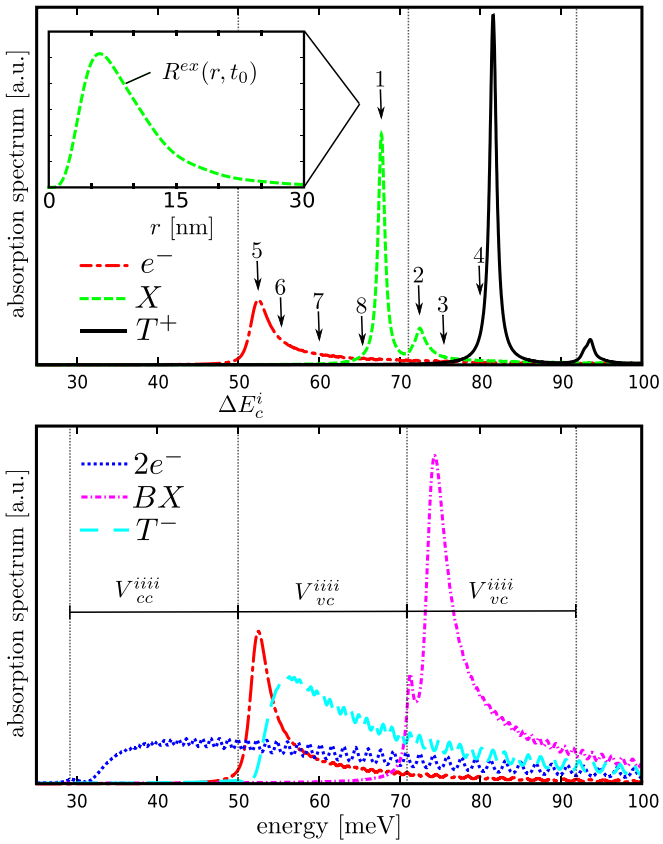

FIG. 3. (Color online) Intraband absorption spectra for several initial occupations $|c\rangle$ depicted in Fig. 1. The QD is initially occupied by e^-: single electron (Coulomb free), X: exciton, $2e^-$: two electrons, BX: biexciton, T^-: negative charged trion; and T^+: positive charged trion. The spectra are shifted and show signatures (e.g., a splitting) of an bound-to-continuum exciton due to Coulomb interaction. The arrows describe the excitation energy of the spectrally narrow pulses, used in Fig. 4. The inset shows $|R^{\rm ex}(r,t_0)|^2 r^2$ the radial occupation property for excitation pulse 1.

induced effects are present in the intraband absorption spectra: (i) spectral shifts of the spectrum, (ii) the formation of a bound exciton[3] between a hole in the QD and an electron in the continuum, and (iii) changes in the width of the absorption continuum.

We start with a discussion of (i) the Coulomb-induced shifts: In comparison to the single-electron spectrum e^- not influenced by Coulomb components all other spectra show a Coulomb-induced shift. The attractive Coulomb interaction between bound electrons and holes inside the QD forms an exciton with a binding energy of $V_{vc}^{iiii} = 21.6$ meV, which is in a good agreement with Ref. [13]. This leads to a spectral shift to higher energies for the bound-to-continuum transition, clearly visible in the exciton spectrum X in Fig. 3. These shifts are also present for all initial configurations with an occupied hole state. Correspondingly, the repulsive contribution between bound electrons inside the QD $V_{cc}^{iiii} = 21.3$ meV results in a shift to lower energies, e.g., two-electron spectrum $2e^-$ in Fig. 3.

Second, we discuss (ii) the formation of a bound exciton between an hole in the QD and an electron in the continuum: Attractive electron-hole interactions between a hole in the QD and an electron in the continuum $V_{vc}^{i\mathbf{k}'\mathbf{k}i}$ lead to the formation of bound excitons. The attractive Coulomb interaction between the bound hole and continuum electron causes a binding of the continuum electron to the QD on a larger spatial scale than bound electrons. Since the small spatial scale of the confinement potential determines the spatial extension of bound electrons.

The formed bound excitons are visible in the spectra by a splitting at the continuum edge (see the exciton X, positive charged trion T^+, and biexciton BX spectra in Fig. 3). The peaks near or below the conduction band edge are the resonances of the lowest-energy bound state of the bound-to-continuum exciton. In Fig. 3 the spectrum for exciton X, biexciton BX, and positive charges trion T^+ show various splitting strengths. The strongest splitting exists in the spectrum of the positive trion T^+ because there are two holes and no additional electron in the QD, this configuration increases the influence of the attractive exciton-forming Coulomb processes. To get information about the relevant properties of the bound-to-continuum excitons, we excite the system in the simulation with spectrally narrow pulses to excite selectively the different exciton states. The different pulse energies are depicted by arrows in Fig. 3. We assume that as a result only one bound-to-continuum intraband exciton is mainly excited. The other excitons like the higher-energy delocalized exciton may be partly also excited, but the influence of these contributions is probably very small. Therefore this approach should extract the essential properties of the state anyway. The bound-to-continuum exciton wave function $\phi^{\rm ex}(\mathbf{r},t_0) = Y_1^0(\vartheta,\varphi)R^{\rm ex}(r,t_0)$ at the time t_0 present after the test pulse can be approximated by:

$$R^{\rm ex}(r,t_0) = \sum_{\mathbf{k}} \langle 1,0,0,1|\rho|\mathbf{k}\uparrow\rangle(t_0) R_{\mathbf{k}}^{\rm bulk}(r). \qquad (11)$$

To get information about the localization of the particle the probability $|R^{\rm ex}(r,t_0)|^2 r^2$ is depicted in Fig. 4 for several excitation energies. There, we compare the results for the configuration with a single electron e^- not influenced by Coulomb processes and for the initial configuration with one exciton X affected by the basic Coulomb contribution that forms bound-to-continuum excitons.

For excitation frequency 1 (slightly before the continuum edge) and 2 (a little above the continuum edge) the Coulomb coupling leads to a formation of a bound state for the QD initially occupied by an exciton X. (See, for example, the plots of the spatial electron probability in the inset of Figs. 3 and 4 for excitation positions 1 and 2.) Here the electron is located in and in the vicinity of the QD: The localized electron is staying at distances between 0 and 15 nm for excitation at frequency 1 and between 0 and 100 nm for excitation at frequency 2. Comparing these values to the size of the QD $\Delta_{\rm QD} = 10$ nm we recognize that the electron is extended in a much larger area around the QD, especially for the energetically higher states.

[3]In fact, it is only a bound-to-continuum exciton if initially an exciton is present. For the trion or biexciton cases, we should call it bound-to-continuum trions or biexcitons, respectively. However, to keep the language simple, we still call them all excitons in the text.

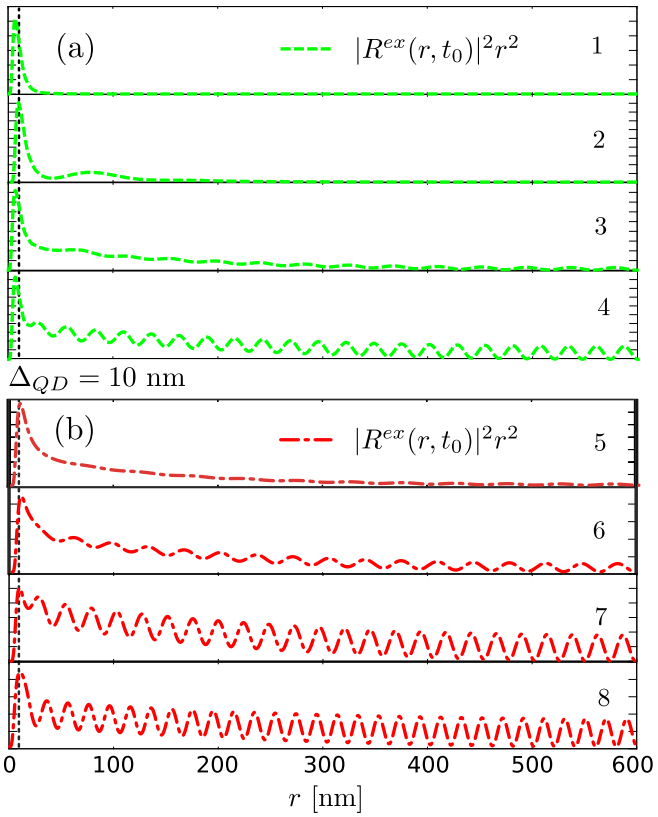

FIG. 4. (Color online) The spatial radial exciton probability $|R^{ex}(r,t_0)|^2 r^2$ for several excitation energies, cf. arrows in Fig. 3. (a) The initial exciton configuration X is influenced by Coulomb processes. (b) Initially occupied with a single electron e^- the system is not influenced by Coulomb processes. Due to the attractive Coulomb coupling a bound exciton state is formed, cf. inset of Fig. 3. The extension of the QD is marked by $\Delta_{QD} = 10$ nm.

If the excitation occurs at higher energies, the electronic wave function is delocalized over the entire area. Therefore, the states are unbound and free (cf. excitation positions 3 and 4 in Fig. 4).

Without the influence of Coulomb interaction in the case of a single electron e^- the state is not really bound to the QD compared to the Coulomb bound states in Fig. 4 for excitation at positions 1 and 2. Here, the excitation at the peak 5 results in a state that has more probability to be located at the QD compared to the outside (free particle), but it is still delocalized over the whole space (cf. Fig. 4). The higher the excitation energy is, the more the electron is equally delocalized over the entire space (cf. Fig. 4 for excitation at positions 6, 7, and 8).

Finally, we discuss (iii) the Coulomb induced changes in the width of the absorption continuum: The Coulomb interaction between the bound and continuum carriers creates energy shifts and causes the formation of excitons. For both mechanisms the effect depends on the different involved continuum states. This leads to a redistribution of oscillator strength in the spectrum. The redistribution of the oscillator strength is visible in the spectrum by a changed width of the absorption spectrum.

Carriers of the continuum are for higher eigenenergies of the single-particle states less located in the quantum dot [cf. Fig. 4(b)], thus the Coulomb effects between bound and continuum carriers are smaller for continuum states with higher energies. Consequently, attractive (repulsive) interaction of the continuum electron with a bound hole (electron) leads to a decreased (increased) broadening. Therefore, compared to the Coulomb free single-electron spectrum e^- in Fig. 3, the absorption continuum is broadened (narrowed) for additional negative (positive) bound carriers. Additional negative carriers and thus a increased broadening can be found for the initial configurations of two electrons $2e^-$, a negative charged trion T^-, and a biexciton BX. The decrease in broadening, compared to the case with one electron present, is found for configurations with additional positive carriers (an exciton X, a positive charged trion T^+, and a biexciton BX). The increase of the linewidth is mainly recognizable in the two electron spectrum $2e^-$ in Fig. 3. The most prominent example for a decrease in linewidth is visible in the positive trion case (cf. Fig. 3).

In conclusion, we present bound-to-continuum intraband absorption spectra including the Coulomb interaction between QD and continuum carriers (bulk or wetting layer). Several configurations of the initial occupations of the QD are studied, resulting in characteristic spectral signatures. In particular, we present signatures of excitons consisting of a localized carrier inside the QD and a delocalized carrier of the continuum.

We thank Andreas Knorr and Sverre Theuerholz for insightful discussions. We also acknowledge Nina Owschimikow, Mirco Kolarczik, and Ulrike Woggon for fruitful discussions. Financial support by Deutsche Forschungsgemeinschaft (DFG) through Sonderforschungsbereich 787 (Project No. B1) is gratefully acknowledged.

[1] L. Brahim and M. Orrit, Rep. Prog. Phys. **68**, 1129 (2005).
[2] D. Bimberg, E. Stock, A. Lochmann, A. Schliwa, J. A. Tofflinger, W. Unrau, M. Munnix, S. Rodt, V. A. Haisler, A. I. Toropov, A. Bakarov, and A. K. Kalagin, IEEE Photonics J. **1**, 58 (2009).
[3] Q. Qiao, B. H. Li, C. Shan, J. S. Liu, J. Yu, X. H. Xie, Z. Z. Zhang, T. B. Ji, Y. Jia, and D. Z. Shen, Mater. Lett. **74**, 104 (2012).
[4] K. J. Vahala, Nature (London) **424**, 839 (2003).
[5] K. A. Piegdon, M. Offer, A. Lorke, M. Urbanski, A. Hoischen, H.-S. Kitzerow, S. Declair, J. Förstner, T. Meier, D. Reuter, A. D. Wieck, and C. Meier, Phys. E (Amsterdam, Neth.) **42**, 2552 (2010).
[6] X. Song, S. Declair, T. Meier, A. Zrenner, and J. Förstner, Opt. Express **20**, 14130 (2012).
[7] I. Robert-Philip, E. Moreau, S. Varoutsis, J. Bylander, M. Gallart, J. M. Gérard, and I. Abram, J. Lumin. **102-103**, 67 (2003).

[8] E. Stock, M.-R. Dachner, T. Warming, A. Schliwa, A. Lochmann, A. Hoffmann, A. I. Toropov, A. K. Bakarov, I. A. Derebezov, M. Richter, V. A. Haisler, A. Knorr, and D. Bimberg, Phys. Rev. B **83**, 041304 (2011).
[9] W. H. Jiang, H. Z. Xu, B. Xu, X. L. Ye, J. Wu, D. Ding, J. B. Liang, and Z. G. Wang, J. Cryst. Growth **212**, 356 (2000).
[10] R. L. Sellin, C. Ribbat, M. Grundmann, N. N. Ledentsov, and D. Bimberg, Appl. Phys. Lett. **78**, 1207 (2001).
[11] A. F. Tsatsul'nikov, A. R. Kovsh, A. E. Zhukov, Y. M. Shernyakov, Y. G. Musikhin, V. M. Ustinov, N. A. Bert, P. S. Kop'ev, Z. I. Alferov, A. M. Mintairov, J. L. Merz, N. N. Ledentsov, and D. Bimberg, J. Appl. Phys. **88**, 6272 (2000).
[12] N. N. Ledentsov, V. A. Shchukin, M. Grundmann, N. Kirstaedter, J. Böhrer, O. Schmidt, D. Bimberg, V. M. Ustinov, A. Y. Egorov, A. E. Zhukov, P. S. Kop'ev, S. V. Zaitsev, N. Y. Gordeev, Z. I. Alferov, A. I. Borovkov, A. O. Kosogov, S. S. Ruvimov, P. Werner, U. Gösele, and J. Heydenreich, Phys. Rev. B **54**, 8743 (1996).
[13] O. Stier, M. Grundmann, and D. Bimberg, Phys. Rev. B **59**, 5688 (1999).
[14] A. D. Yoffe, Adv. Phys. **50**, 1 (2001).
[15] J. Huneke, I. D'Amico, P. Machnikowski, T. Thomay, R. Bratschitsch, A. Leitenstorfer, and T. Kuhn, Phys. Rev. B **84**, 115320 (2011).
[16] A. Steinhoff, H. Kurtze, P. Gartner, M. Florian, D. Reuter, A. D. Wieck, M. Bayer, and F. Jahnke, Phys. Rev. B **88**, 205309 (2013).
[17] M. Lorke, F. Jahnke, and W. W. Chow, Appl. Phys. Lett. **90**, 051112 (2007).
[18] A. Carmele, A. Knorr, and M. Richter, Phys. Rev. B **79**, 035316 (2009).
[19] J. Gomis-Bresco, S. Dommers, V. V. Temnov, U. Woggon, M. Laemmlin, D. Bimberg, E. Malic, M. Richter, E. Schöll, and A. Knorr, Phys. Rev. Lett. **101**, 256803 (2008).
[20] R. Ferreira and G. Bastard, Nanoscale Res. Lett. **1**, 120 (2006).
[21] P. Lelong, S.-W. Lee, K. Hirakawa, and H. Sakaki, Phys. E (Amsterdam, Neth.) **7**, 174 (2000).
[22] Y. Harada, T. Maeda, and T. Kita, J. Appl. Phys. **113**, 223511 (2013).
[23] A. Marti, E. Antolin, C. R. Stanley, C. D. Farmer, N. Lopez, P. Diaz, E. Canovas, P. G. Linares, and A. Luque, Phys. Rev. Lett. **97**, 247701 (2006).
[24] D. Wasserman, T. Ribaudo, S. A. Lyon, S. K. Lyo, and E. A. Shaner, Appl. Phys. Lett. **94**, 061101 (2009).
[25] A. Barve, S. Lee, S. Noh, and S. Krishna, Laser Photonics Rev. **4**, 738 (2010).
[26] N. H. Kwong, R. Binder, and M. Lindberg, Opt. Lett. **29**, 2536 (2004).
[27] S. C. Kuhn, A. Knorr, M. Richter, N. Owschimikow, M. Kolarczik, Y. I. Kaptan, and U. Woggon, Phys. Rev. B **89**, 201414 (2014).
[28] A. Luque, A. Martí, A. Mellor, D. Fuertes Marrón, I. Tobías, and E. Antolín, Progress in Photovoltaics: Research and Applications **21**, 658 (2013).
[29] T. Kita, T. Maeda, and Y. Harada, Phys. Rev. B **86**, 035301 (2012).
[30] S. Sauvage, P. Boucaud, J.-M. Gérard, and V. Thierry-Mieg, Phys. Rev. B **58**, 10562 (1998).
[31] W. P. Dumke, Phys. Rev. **124**, 1813 (1961).
[32] J. Kabuss, S. Werner, A. Hoffmann, P. Hildebrandt, A. Knorr, and M. Richter, Phys. Rev. B **81**, 075314 (2010).
[33] N. Owschimikow, M. Kolarczik, Y. I. Kaptan, N. B. Grosse, and U. Woggon, Appl. Phys. Lett. (to be published).
[34] F. Quochi, M. Dinu, L. N. Pfeiffer, K. W. West, C. Kerbage, R. S. Windeler, and B. J. Eggleton, Phys. Rev. B **67**, 235323 (2003).
[35] G. Dasbach, T. Baars, M. Bayer, A. Larionov, and A. Forchel, Phys. Rev. B **62**, 13076 (2000).
[36] S. Dommers, V. V. Temnov, U. Woggon, J. Gomis, J. Martinez-Pastor, M. Laemmlin, and D. Bimberg, Appl. Phys. Lett. **90**, 033508 (2007).
[37] H. Haug and S. Koch, *Quantum Theory of the Optical and Electronic Properties of Semiconductors*, 5th ed. (World Scientific, Singapore, 2009).
[38] B. Gu, N. H. Kwong, and R. Binder, Phys. Rev. B **87**, 125301 (2013).
[39] B. Krummheuer, V. M. Axt, and T. Kuhn, Phys. Rev. B **65**, 195313 (2002).
[40] S. Rudin and T. L. Reinecke, Phys. Rev. B **66**, 085314 (2002).
[41] COMSOL MULTIPHYSICS 4.3B, www.comsol.com.
[42] E. A. Muljarov and R. Zimmermann, Phys. Rev. Lett. **98**, 187401 (2007).
[43] H. C. Schneider, W. W. Chow, and S. W. Koch, Phys. Rev. B **64**, 115315 (2001).
[44] B. T. Miller, W. Hansen, S. Manus, R. J. Luyken, A. Lorke, J. P. Kotthaus, S. Huant, G. Medeiros-Ribeiro, and P. M. Petroff, Phys. Rev. B **56**, 6764 (1997).
[45] E. A. Muljarov and R. Zimmermann, Phys. Rev. Lett. **93**, 237401 (2004).